Available online at www.sciencedirect.com

ScienceDirect

IFAC PapersOnLine 51-31 (2018) 967–972

Piecewise Affine H_∞ Control of Half-Car Magneto-Rheological Suspension Systems

Jian Wu * **Zhiyuan Liu** *

* *Department of Control Science and Engineering, Harbin Institute of Technology, Harbin, China (e-mail:vijaychn217@gmail.com, liuzy_hit@hit.edu.cn).*

Abstract: This paper presents a novel controller design for half-car magneto-rheological (MR) suspension systems. By introducing a piecewise approximation model, the nonlinear constraints of MR dampers are transformed into piecewise constant constraints. Further, by defining a piecewise affine control law, the attenuation of pitch and heave responses are realized by satisfying a given H_∞ index. The control gains are derived through linear-matrix-inequality (LMI) optimization. Simulations under random and impact roads have verified the effectiveness of proposed controller on performance improvement and constraint satisfaction.

© 2018, IFAC (International Federation of Automatic Control) Hosting by Elsevier Ltd. All rights reserved.

Keywords: Semi-active suspension, half-car model, magneto-rheological damper, H_∞ control.

1. INTRODUCTION

A typical automotive suspension must provides ride comfort in view of road roughness inputs and secures good road handling property. Conventional passive suspensions always suffer conflict from these two requirements, which has resulted in massive researches and attempts in the area of active and semi-active suspensions (Tseng and Hrovat (2015)). Active suspensions can offer opportunities for substantial improvements in ride and handling as well as overall vehicle posture, but high energy consumption, cost and complexity are requested with pumps or compressors (Huang et al. (2018)). Semi-active suspensions can improve the comfort and handling performance by only adjust the damping properties with acceptable energy consumption and compact actuator size, which are applicable and promising.

Among the existing semi-active actuators, magnetorheological (MR) dampers, which can change its damping with different applied current, have drawn more attentions from the academic and industrial circles due to their fast response and highly adjustable range (Choi et al. (2016)). However, many researches have shown that MR dampers have complex dynamics, for example, the hysteresis, biviscous and energy dissipativity (Wang and Liao (2011)). Thus, the task of controller design while considering the actuator dynamics has been a hot issue.

Skyhook control or its modified styles have been widely used in the industrial area (Choi et al. (2001)), where an ideal damper that connects the vehicle body and the 'sky' is set as a desired closed-loop property. To further explore a control method with higher performance, many control theories, such as LQR/LQG, H_∞, sliding mode and so on, have been employed. For example, Du et al. (2005) has firstly design a static H_∞ controller for an active suspension, and then the active control force is realized with the MR damper using a designed polynomial model. In Pohoryles and Duffour (2015), the active damping force is designed by LQG control, and a new rule to obtain the current value is derived by analyzing the dynamics of MR dampers under different excitation frequencies. However, these methods have neglected the dynamics of MR dampers during the design of damping force, thus the proposed results are 'clipped optimal'. To consider the complex actuator nonlinearities, some control algorithms have been given based on the MPC technique. For example, by designing a hybrid MPC controller to approach the optimal semi-active suspension, Giorgetti et al. (2006) has shown that significant deviation of optimal from the 'clipped optimal' can occur. To realize the online application, Canale et al. (2006) and Csek et al. (2015) have explored a 'fast' MPC method and an neural network approximation of MPC laws, respectively.

Considering the above problems, a static H_∞ controller which can be easily applied has been given in this paper based on a piecewise approximation of the suspension model. Additionally, differ from the above MPC methods which only consider a quarter-car model, this paper studies the attenuation of pitch and heave motions with a half-car model. The nonlinear actuator constraints are approximated by piecewise constant constraints and the system state space is divided by a certain number of partitions based on the vibration velocities of front and rear suspensions. This paper is organized as follows. Section 2 gives the half-car suspension model and the nonlinear actuator constraints. The model approximation and controller design are given in Section 3. Section 4 gives the simulation results and analysis under different road profiles.

2. PROBLEM STATEMENT

2.1 Half-Car Suspension System

A half-car MR suspension model is shown in Fig. 1 where F_{fmr} and F_{rmr} are damping forces produced by the MR

⋆ This work is support by China Automobile Industry Innovation and Development Joint Fund (No.U1564213).

2405-8963 © 2018, IFAC (International Federation of Automatic Control) Hosting by Elsevier Ltd. All rights reserved.
Peer review under responsibility of International Federation of Automatic Control.
10.1016/j.ifacol.2018.10.055

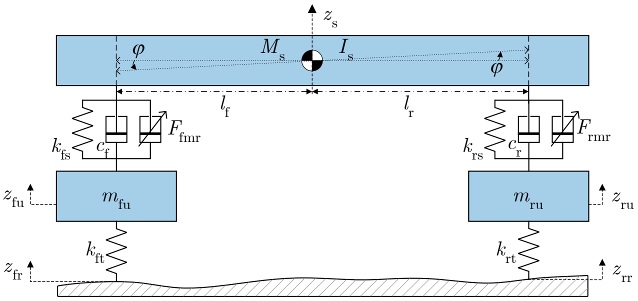

Fig. 1. Half-car MR suspension systems

dampers. The dynamics of the sprung mass (M_s) and unsprung masses (m_{fu} and m_{ru}) can be described as follows

$$\begin{aligned}&M_s\ddot{z}_s = -F_{fmr} - F_{rmr} - F_{fs} - F_{rs} - F_{fd} - F_{rd},\\&I_s\ddot{\varphi} = l_f(F_{fd} + F_{fs} + F_{fmr}) - l_r(F_{rd} + F_{rs} + F_{rmr}),\\&m_{fu}\ddot{z}_{fu} = F_{fmr} + F_{fs} + F_{fd} - F_{ft},\\&m_{ru}\ddot{z}_{ru} = F_{rmr} + F_{rs} + F_{rd} - F_{rt}\end{aligned} \tag{1}$$

where z_s is the vertical displacements of vehicle mass center, I_s and φ stand for the moment of inertia and the pitch angle of vehicle body. The forces in equation (1) produced by springs, passive dampers and tires satisfy

$$\begin{aligned}&F_{fs} = k_{fs}(z_s - l_f\varphi - z_{fu}),\ F_{rs} = k_{rs}(z_s + l_r\varphi - z_{ru}),\\&F_{fd} = c_f(\dot{z}_s - l_f\dot{\varphi} - \dot{z}_{fu}),\ F_{rd} = c_r(\dot{z}_s + l_r\dot{\varphi} - \dot{z}_{ru}),\\&F_{ft} = k_{ft}(z_{fu} - z_{fr}),\qquad F_{rt} = k_{rt}(z_{ru} - z_{rr})\end{aligned} \tag{2}$$

where k_{fs} and k_{rs} are the spring stiffness; c_f and c_r are the damping coefficients of passive dampers; k_{ft} and k_{rt} are the equivalent stiffness of pneumatic tires; z_{fu} and z_{ru} stand for the vertical displacements of unsprung masses; z_{fr} and z_{rr} are the excitations from uneven road profiles.

2.2 Nonlinear Actuator Constraints

In equation (1), F_{fmr} and F_{rmr} have complicate relationship with the driving current I and the deflection conditions of MR dampers, which can be generally described by a modified Bouc-Wen model as follows

$$\begin{aligned}&F_{mr} = c_1\dot{\xi} + k_1(\chi - \chi_0),\\&\dot{\xi} = \frac{1}{c_0 + c_1}[\alpha\varpi + c_0\dot{\chi} + k_0(\chi - \xi)],\\&\dot{\varpi} = -\gamma|\dot{\chi} - \dot{\xi}||\varpi|^{n-1}\varpi - \beta(\dot{\chi} - \dot{\xi})|\varpi|^n + k_2(\dot{\chi} - \dot{\xi})\end{aligned} \tag{3}$$

where F_{mr} and χ are the damping force and stroke of MR dampers, respectively (referring to (1), $F_{mr} = F_{fmr}$ or F_{rmr} and $\chi = z_s - l_f\varphi - z_{fu}$ or $z_s + l_r\varphi - z_{ru}$); ξ and ϖ are the inertial variables. Furthermore, model (3) has ten parameters which form a parameter set $\Phi = [c_0, c_1, k_0, k_1, k_2, \alpha, \beta, \gamma, \chi_0, n]$ where α, c_0 and c_1 satisfy linear or nonlinear relationships with I.

Due to the complexity shown in (3), it is difficult to design a controller directly based on a model consists of (1) and (3). Therefore, a practical method generally consists of two steps. In the first step, a controller is designed based on (1) to give desired damping forces, and in the second step, the forces are transformed into current values based on calculations of MR damper models or static MAPs. However, in the first step, the capacity of MR dampers should be totally concerned. Otherwise, the desired forces will be impossible to be tracked through the second step, and the designed performance will not be guaranteed.

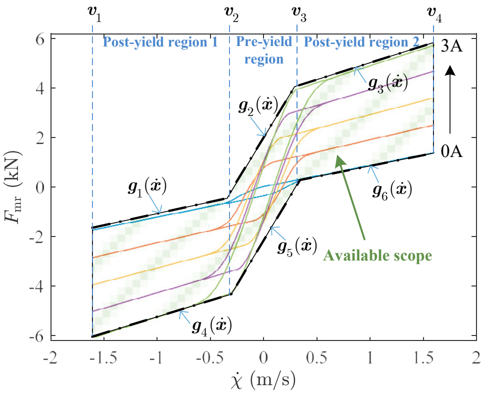

Fig. 2. Force/velocity characteristics of MR dampers

Fig. 2 shows the simulation results of model (3) under sinusoidal excitations and varied current values, where the nonlinear dynamics of MR dampers, including hysteresis, bilinear and energy dissipation characters, are revealed under the force/velocity coordinate system. Meanwhile, Fig. 2 also shows the available scope of the damping force. In this paper, the envelope of the available scope is described with six straight lines as follows

$$g_k(\dot{\chi}) = a_k + b_k\dot{\chi}, \quad k = 1, \ldots, 6. \tag{4}$$

Further, by defining the endpoints of these lines as $v_i, i = 1, \ldots, 4$, the bounds of the available scope can be obtained as follows

$$g_{u\,(\text{or}\,l)}(\dot{\chi}) = \begin{cases} g_{1\,(\text{or}\,4)}(\dot{\chi}) & v_1 \le \dot{\chi} < v_2\\ g_{2\,(\text{or}\,5)}(\dot{\chi}) & v_2 \le \dot{\chi} \le v_3\\ g_{3\,(\text{or}\,6)}(\dot{\chi}) & v_3 < \dot{\chi} \le v_4\end{cases} \tag{5}$$

where g_u stands for the upper bound and g_l is the lower bound. Based on (5), the nonlinear constraints on F_{fmr} and F_{rmr} can be described as follows

$$\begin{aligned}&g_l(\dot{z}_s - l_f\dot{\varphi} - \dot{z}_{fu}) \le F_{fmr} \le g_u(\dot{z}_s - l_f\dot{\varphi} - \dot{z}_{fu}),\\&g_l(\dot{z}_s + l_r\dot{\varphi} - \dot{z}_{ru}) \le F_{rmr} \le g_u(\dot{z}_s + l_r\dot{\varphi} - \dot{z}_{ru}).\end{aligned} \tag{6}$$

2.3 Problem Statement

Define the state vector of system as

$$\begin{aligned}&x = [x_1\ \ x_2\ \ x_3\ \ x_4\ \ x_5\ \ x_6\ \ x_7\ \ x_8]^T,\\&x_1 = z_s - l_f\varphi - z_{fu},\quad x_2 = z_s + l_r\varphi - z_{ru},\\&x_3 = z_{fu} - z_{fr},\quad x_4 = z_{ru} - z_{rr},\quad x_5 = \dot{z}_s - l_f\dot{\varphi},\\&x_6 = \dot{z}_s + l_r\dot{\varphi}\quad x_7 = \dot{z}_{fu},\quad x_8 = \dot{z}_{ru}.\end{aligned} \tag{7}$$

Then, by defining the control input as $u = [F_{fmr}\ F_{rmr}]^T$, the disturbance input as $w = [\dot{z}_{fr}\ \dot{z}_{rr}]^T$ and the performance output as $z = [\rho_1\ddot{z}_s\ \rho_2\ddot{\varphi}]^T$, expression (1) can be written in a state space equation as follows

$$\begin{aligned}&\dot{x} = Ax + Bu + Ew,\\&z = Cx + Du\end{aligned} \tag{8}$$

where

$$A = \begin{bmatrix} 0 & 0 & 0 & 0 & 1 & 0 & -1 & 0\\ 0 & 0 & 0 & 0 & 0 & 1 & 0 & -1\\ 0 & 0 & 0 & 0 & 0 & 0 & 1 & 0\\ 0 & 0 & 0 & 0 & 0 & 0 & 0 & 1\\ -\epsilon_1 k_{fs} & -\epsilon_2 k_{rs} & 0 & 0 & -\epsilon_1 c_f & -\epsilon_2 c_r & \epsilon_1 c_f & \epsilon_2 c_r\\ -\epsilon_2 k_{fs} & -\epsilon_3 k_{rs} & 0 & 0 & -\epsilon_2 c_f & -\epsilon_3 c_r & \epsilon_2 c_f & \epsilon_3 c_r\\ \frac{k_{fs}}{m_{fu}} & 0 & -\frac{k_{ft}}{m_{fu}} & 0 & \frac{c_f}{m_{fu}} & 0 & -\frac{c_f}{m_{fu}} & 0\\ 0 & \frac{k_{rs}}{m_{ru}} & 0 & -\frac{k_{rt}}{m_{ru}} & 0 & \frac{c_r}{m_{ru}} & 0 & -\frac{c_r}{m_{ru}} \end{bmatrix}$$

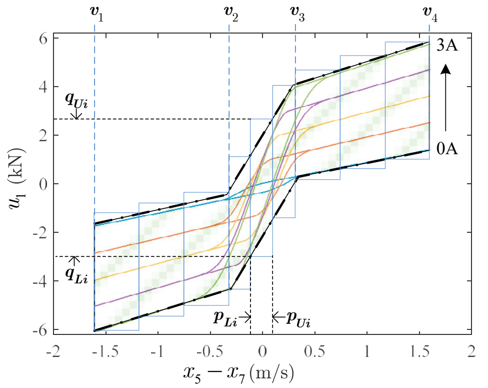

Fig. 3. Piecewise approximation of the available scope

$$B = \begin{bmatrix} 0_{4\times1} & 0_{4\times1} \\ -\epsilon_1 & -\epsilon_2 \\ -\epsilon_2 & -\epsilon_3 \\ 1/m_{\mathrm{fu}} & 0 \\ 0 & 1/m_{\mathrm{ru}} \end{bmatrix}, E = \begin{bmatrix} 0 & 0 \\ 0 & 0 \\ -1 & 0 \\ 0 & -1 \\ 0_{4\times1} & 0_{4\times1} \end{bmatrix},$$

$$C = \begin{bmatrix} -\dfrac{\rho_1}{M_{\mathrm{s}}} & 0 \\ 0 & \dfrac{\rho_2}{I_{\mathrm{s}}} \end{bmatrix} \begin{bmatrix} k_{\mathrm{fs}} & k_{\mathrm{rs}} & 0 & 0 & c_{\mathrm{f}} & c_{\mathrm{r}} & -c_{\mathrm{f}} & -c_{\mathrm{r}} \\ l_{\mathrm{f}}k_{\mathrm{fs}} & -l_{\mathrm{r}}k_{\mathrm{rs}} & 0 & 0 & l_{\mathrm{f}}c_{\mathrm{f}} & -l_{\mathrm{r}}c_{\mathrm{r}} & -l_{\mathrm{f}}c_{\mathrm{f}} & l_{\mathrm{r}}c_{\mathrm{r}} \end{bmatrix},$$

$$D = \left[-\frac{\rho_1}{M_{\mathrm{s}}} \;\; -\frac{\rho_1}{M_{\mathrm{s}}};\; \frac{\rho_2 l_{\mathrm{f}}}{I_{\mathrm{s}}} \;\; -\frac{\rho_2 l_{\mathrm{r}}}{I_{\mathrm{s}}}\right],$$

$$\epsilon_1 = \frac{1}{M_{\mathrm{s}}} + \frac{l_{\mathrm{f}}^2}{I_{\mathrm{s}}},\ \epsilon_2 = \frac{1}{M_{\mathrm{s}}} - \frac{l_{\mathrm{f}}l_{\mathrm{r}}}{I_{\mathrm{s}}},\ \epsilon_3 = \frac{1}{M_{\mathrm{s}}} + \frac{l_{\mathrm{r}}^2}{I_{\mathrm{s}}}.$$

Further, the nonlinear constraints in (6) can be written as

$$\begin{aligned} g_{\mathrm{l}}(x_5 - x_7) \le u_1 \le g_{\mathrm{u}}(x_5 - x_7), \\ g_{\mathrm{l}}(x_6 - x_8) \le u_2 \le g_{\mathrm{u}}(x_6 - x_8). \end{aligned} \tag{9}$$

Above all, the main task of this paper is to design control inputs u_i $(i = 1, 2)$ such that system (8) is asymptotically stable and the H_∞ norm from w to z is less than a given scalar γ. In addition, the nonlinear state-dependent constraints in (9) should be satisfied.

3. PIECEWISE AFFINE H_∞ CONTROLLER SYNTHESIS

To handle the nonlinear constraints in (9), existing research always appeal to MPC techniques which face large calculation burden. Therefore, this paper will consider a static H_∞ control method based on a piecewise model approximation technique.

3.1 Transformation to Constrained Piecewise Systems

As shown in Fig. 3 which takes the MR damper of front axle as a example, the available scope can be approximated by 9 strip-shaped partitions (3 partitions for each of the three different damping regions: pre-yield region, post-yield regions 1 and 2). Define $i = 1, \ldots, 9$ as the partition index of front axle, p_{Li} and p_{Ui} as the lower and upper velocity bounds of the i-th partition, then we have

$$p_{Li} = \begin{cases} v_1 + (v_2 - v_1)(i-1)/3 & 1 \le i \le 3 \\ v_2 + (v_3 - v_2)(i-4)/3 & 3 < i \le 6 \\ v_3 + (v_4 - v_3)(i-7)/3 & 6 < i \le 9, \end{cases} \tag{10}$$

$$p_{Ui} = \begin{cases} v_1 + (v_2 - v_1)i/3 & 1 \le i \le 3 \\ v_2 + (v_3 - v_2)(i-3)/3 & 3 < i \le 6 \\ v_3 + (v_4 - v_3)(i-6)/3 & 6 < i \le 9. \end{cases} \tag{11}$$

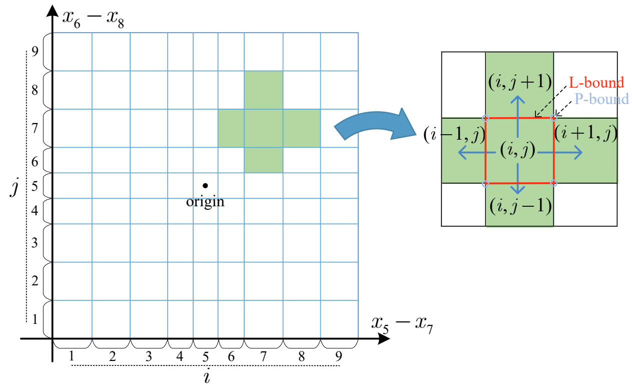

Fig. 4. System partitions and state transition

Further, we use two constant values to approximate the nonlinear control constraint in each partition. Specifically, by define q_{Li} and q_{Ui} as the damping force constraints of i-th partition and referring to (5), (10) and (11), we can obtain the expression for q_{Li} and q_{Ui} as follows

$$q_{Li} = \begin{cases} g_{\mathrm{l}}(p_{Li}) & i \ne 5 \\ (g_{\mathrm{l}}(p_{Li}) - g_{\mathrm{u}}(p_{Ui}))/2 & i = 5, \end{cases} \tag{12}$$

$$q_{Ui} = \begin{cases} g_{\mathrm{u}}(p_{Ui}) & i \ne 5 \\ (g_{\mathrm{u}}(p_{Ui}) - g_{\mathrm{l}}(p_{Li}))/2 & i = 5. \end{cases} \tag{13}$$

Based on the above approximation, the nonlinear control constraint of front axle has been transformed into piecewise linear constraints. Furthermore, benefiting from the symmetry of the actuator dynamics in the first and third quadrants of the velocity/force coordinate system, we can choose the values of v_2 and v_3 such that $v_2 = -v_3$. Then, we can guarantee that the system origin $(x = 0)$ will not located in any boundaries of the partitions and the constraints in origin-included partition $(i = 5)$ are symmetrical, thus $q_{L5} = q_{U5}$.

Similarly, by defining $j = 1, \ldots, 9$ as the partition index of rear axle, we can obtain the velocity bounds p_{Lj} and p_{Uj}, and the corresponding control constraints q_{Lj} and q_{Uj}.

By using the above approximation technique and choosing appropriate sample time and a discretization method, (8) and (9) can be transformed into a combination of the following discrete-time subsystems

$$\begin{aligned} &x(k+1) = A_{i,j}x(k) + B_{i,j}u(k) + E_{i,j}w(k), \\ &z(k) = C_{i,j}x(k) + D_{i,j}u(k), \\ &u(k) \in \mathcal{S}_{i,j}, \quad x(k) \in \mathcal{R}_{i,j} \end{aligned} \tag{14}$$

where $\mathcal{R}_{i,j} := \{x(k) | p_{Li} \le x_5(k) - x_7(k) \le p_{Ui}, p_{Lj} \le x_6(k) - x_8(k) \le p_{Uj}\}$ is the defined state domain and $\mathcal{S}_{i,j} := \{u(k) | q_{Li} \le u_1(k) \le q_{Ui}, q_{Lj} \le u_2(k) \le q_{Uj}\}$ is the control constraint of the (i, j)-th subsystem.

Fig. 4 shows the state domain of all subsystems. It is easy to see that there will be 81 subsystems when the available scope of each MR damper is divided into 9 partitions. Further, Fig. 4 has also taken the (i, j)-th domain as an example to show the possible state transition. Thus, the boundary of any two domains where the state transition may happen is assumed to be a line (L-bounds in Fig. 4) but not a single point (P-bounds in Fig. 4). In applications, when the state unfortunately pass through the P-bounds, this assumption is easy to be realized by adding a small offset to the state value. In addition, when the system state transits from $\mathcal{R}_{i,j}$ to domain $\mathcal{R}_{m,n}$ at the time k, we specify that the system is governed by the dynamics of the subsystem in $\mathcal{R}_{i,j}$ at that time. Above all, let Ω represent the set of index pairs which denote the possible switch from one partition to itself or another partition, that is

$$\Omega = \{((i,j),(m,n)) | x(k) \in \mathcal{R}_{i,j}, x(k+1) \in \mathcal{R}_{m,n}\} \quad (15)$$

Therefore, the control problem in section 2.3 has been transformed into: design control inputs $u_i (i = 1, 2)$ such that subsystems in (14) are stable and the H_∞ performance is satisfied for all of the state transition defined in (15). In addition, the constant constraints in each partition should be satisfied.

Remark 1. The approximation quality can be enhanced by employing more partitions, however the system and control design will become more complex. So, this paper has taken 9 partitions for each MR damper as an example, but the approximation technique and the following control method are not limited to this.

3.2 Design of a Piecewise Affine H_∞ Controller

From Fig. 3, it is obviously that the control constraints in (14) are mostly asymmetric about zero (except for the origin-included partition $\mathcal{R}_{5,5}$), thus $q_{Li} \neq -q_{Ui}$ and $q_{Lj} \neq q_{Uj}$. However, asymmetrical constraints are always hard to be handled since most of the synthesis methods rely on the concept of invariant set which are ellipsoidal and symmetric. Consider this problem, we employ a piecewise affine control law as follows

$$u(k) = K_{i,j} x(k) + c_{i,j}, \quad i,j = 1, \ldots, 9 \quad (16)$$

where the affine items are pre-designed as $c_{i,j} = [(q_{Li} + q_{Ui})/2 \quad (q_{Lj} + q_{Uj})/2]^T$. Substitute (16) into (14), we can get the closed-loop system as

$$\begin{aligned} & x(k+1) = \bar{A}_{i,j} x(k) + E_{i,j} w(k) + d_{i,j}, \\ & z(k) = \bar{C}_{i,j} x(k) + e_{i,j}, \\ & |(K_{i,j} x(k))_{(\sigma)}| \leq \bar{u}_{i,j(\sigma)}, \quad x(k) \in \mathcal{R}_{i,j} \end{aligned} \quad (17)$$

where $\bar{A}_{i,j} = A_{i,j} + B_{i,j} K_{i,j}$, $\bar{C}_{i,j} = C_{i,j} + D_{i,j} K_{i,j}$, $d_{i,j} = B_{i,j} c_{i,j}$, $e_{i,j} = D_{i,j} c_{i,j}$, $\sigma \in \{1, 2\}$ is the index of row elements, $\bar{u}_{i,j(1)} = (q_{Ui} - q_{Li})/2$ and $\bar{u}_{i,j(2)} = (q_{Uj} - q_{Lj})/2$. Therefore, the asymmetrical control constraints has been transformed into the symmetrical ones on $K_{i,j} x$. Further, as constant items of output equations have no influence on the system stability and H_∞ performance, the control gains $K_{i,j}$ can be equally designed based on the following system

$$\begin{aligned} & x(k+1) = \bar{A}_{i,j} x(k) + E_{i,j} w(k) + d_{i,j}, \\ & z(k) = \bar{C}_{i,j} x(k). \end{aligned} \quad (18)$$

The definition domains $\mathcal{R}_{i,j}$ can be expressed by ellipsoids as follows

$$\mathcal{L}_{i,j} = \{x | \|F_{i,j} x + f_{i,j}\| \leq 1\}, \quad i,j = 1, \ldots, 9 \quad (19)$$

where $F_{i,j(1)} = 2M_{(1)}/(p_{Ui} - p_{Li})$, $F_{i,j(2)} = 2M_{(2)}/(p_{Uj} - p_{Lj})$, $f_{i,j(1)} = -(p_{Li} + p_{Ui})/(p_{Ui} - p_{Li})$, $f_{i,j(2)} = -(p_{Lj} + p_{Uj})/(p_{Uj} - p_{Lj})$, $F_{i,j(1)}$ (or $f_{i,j(1)}$) and $F_{i,j(2)}$ (or $f_{i,j(2)}$) are the first and second row elements of $F_{i,j}$ (or $f_{i,j}$), respectively, and

$$\begin{aligned} M_{(1)} &= [0 \quad 0 \quad 0 \quad 0 \quad 1 \quad 0 \quad -1 \quad 0], \\ M_{(2)} &= [0 \quad 0 \quad 0 \quad 0 \quad 0 \quad 1 \quad 0 \quad -1]. \end{aligned}$$

By specifying the energy bound of $w(k)$ as a known constant, thus $\Sigma_{k=0}^{\infty} \|w(k)\|^2 = w_{\max}$, a theorem to obtain $K_{i,j}$ can be derived as following.

Theorem 1. For the given scalars γ, $w_{\max}$ and all the index pairs $((i,j),(m,n)) \in \Omega$, system (18) is asymptotically stable, the constraints on $K_{i,j} x$ are satisfied and the H_∞ norm from w to z is less than γ, if there exist matrices $Q_{i,j} = Q_{i,j}^T > 0$, $Q_{m,n} = Q_{m,n}^T > 0$, $G_{i,j}$, $R_{i,j}$ and scalars $\eta_{i,j} > 0$, $\mu_{i,j} > 0$ satisfying the following inequalities

$$\begin{bmatrix} -\gamma^2 I & \star & \star & \star & \star \\ E_{i,j} & -Q_{m,n} - \eta_{i,j} d_{i,j} d_{i,j}^T & \star & \star & \star \\ 0 & 0 & -I & \star & \star \\ 0 & \eta_{i,j} f_{i,j} d_{i,j}^T & 0 & -\eta_{i,j}(f_{i,j} f_{i,j}^T - 1) & \star \\ 0 & \Xi_{i,j} & \Gamma_{i,j} & -G_{i,j}^T F_{i,j}^T & \Upsilon_{i,j} \end{bmatrix} < 0, \quad i,j \neq 5, \quad (20)$$

$$\begin{bmatrix} -\gamma^2 I & \star & \star & \star \\ E_{i,j} & -Q_{m,n} & \star & \star \\ 0 & 0 & -I & \star \\ 0 & \Xi_{i,j} & \Gamma_{i,j} & \Upsilon_{i,j} \end{bmatrix} < 0, \quad i,j = 5, \quad (21)$$

$$\begin{bmatrix} \dfrac{\bar{u}_{i,j(\sigma)}^2}{\gamma^2 w_{\max}} \Upsilon_{i,j} & \star & \star \\ \psi_{(\sigma)} R_{i,j} & -I & \star \\ F_{i,j} G_{i,j} & 0 & -\mu_{i,j}(f_{i,j} f_{i,j}^T - 1) \end{bmatrix} < 0, i,j \neq 5, \quad (22)$$

$$\begin{bmatrix} \dfrac{\bar{u}_{i,j(\sigma)}^2}{\gamma^2 w_{\max}} \Upsilon_{i,j} & \star \\ \psi_{(\sigma)} R_{i,j} & -I \end{bmatrix} < 0, \quad i,j = 5 \quad (23)$$

where $\Xi_{i,j} = (A_{i,j} G_{i,j} + B_{i,j} R_{i,j})^T$, $\Gamma_{i,j} = (C_{i,j} G_{i,j} + D_{i,j} R_{i,j})^T$, $\Upsilon_{i,j} = Q_{i,j} - G_{i,j} - G_{i,j}^T$, $\psi_{(1)} = [1 \ 0]$ and $\psi_{(2)} = [0 \ 1]$. Then, the control gains can be derived as

$$K_{i,j} = R_{i,j} G_{i,j}^{-1}. \quad (24)$$

Proof. Due to the limited length and space, the proof is omitted here. Similar techniques used to conclude this theorem can be referred in Gao et al. (2009) where a H_∞ controller is designed for piecewise affine systems with symmetrical control constraints.

Remark 2. In theorem 1, (20) and (21) are used to guarantee the H_∞ performance and system stability, while (22) and (23) are designed for the satisfaction of control constraints. Further, as (20) and (22) can only be used when $f_{i,j} f_{i,j}^T - I > 0$ which is only satisfied for origin-excluded partitions, (21) and (23) have to be specially designed for the origin-included partition.

Remark 3. Based on theorem 1, for the system partitions defined in section 3.1 and the state transition shown in Fig.4, there are totaly 369 inequalities to be solved. This task can be handled by employing a Matlab toolbox named SeDuMi (Sturm (1999)) together with a optimization software named MOSEK. Finally, according to (16), we will obtained an independent affine controller for each of the 81 partitions.

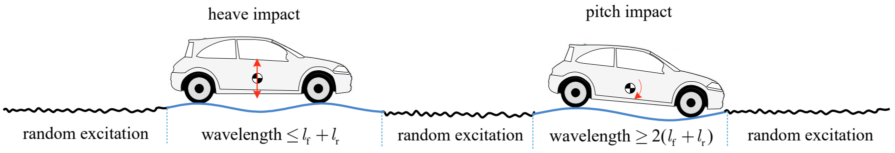

Fig. 5. Simulation road profile consists of random excitations, heave and pitch impacts.

4. SIMULATION ANALYSIS

4.1 Parameters and Environments

To verify that the proposed piecewise affine H_∞ (PWA-H_∞) control design achieves the desired objectives, the resulting closed-loop system has been simulated under different road conditions and compared to both a passive suspension system and an semi-active suspension controlled by classic Skyhook controller. In our simulations, the parameters of the half-car suspension model are listed in Table 1.

Table 1. Parameters of half-car model

Parameter	Value	Parameter	Value
M_s	575kg	l_f	1.38m
$m_{fu} = m_{ru}$	60kg	l_r	1.36m
$k_{fs} = k_{rs}$	16812N/m	I_s	769kg/m^2
$c_f = c_r$	500N/m	$k_{ft} = k_{rt}$	190000N/m

Further, to describe the nonlinearities of MR dampers, a hyperbolic tangent function-based model from Guo et al. (2006) is employed. The model can be expressed as follows

$$F_{\mathrm{mr}} = c_{t0}\dot{\chi} + k_{t0}\chi + y_{\mathrm{mr}} I \tanh(c_{t1}\dot{\chi} + k_{t1}\chi). \qquad (25)$$

According to the test results of a real MR damper from FAW-Tokico Corp., the parameters in (25) can be obtained as c_{t0}=810.78, k_{t0}=620.79, c_{t1}=5.78, k_{t1}=20, and y_{mr}=1200. In the simulation, we assume that F_{fmr} and F_{rmr} both conform to (25). Then, by choosing $-v_1 = v_4$=3m/s and $-v_2 = v_3$=0.4m/s, we can obtain the parameters of the envelope lines in (4) as follows

$$\begin{aligned} &a_1 = 42.31, \quad a_2 = 1836, \quad a_3 = 3635, \; a_4 = -3508, \\ &a_5 = -1762, \; a_6 = -5.989, \; b_1 = 825, \quad b_2 = 5240, \\ &b_3 = 800.6, \quad b_4 = 859.8, \quad b_5 = 5202, \; b_6 = 827.3. \end{aligned}$$

The desired damping forces (F_{fmr} and F_{rmr}) of PWA-H_∞ control are obtained according to (16) and for Skyhook control, the desired damping forces are given as

$$F_{\mathrm{fmr}} = c_{\mathrm{fsky}}(\dot{z}_s - l_f\dot{\varphi}), \quad F_{\mathrm{rmr}} = c_{\mathrm{rsky}}(\dot{z}_s + l_r\dot{\varphi}) \qquad (26)$$

where $c_{\mathrm{fsky}} = c_{\mathrm{rsky}} = 4000$Nm/s. Both the damping forces of PWA-H_∞ and Skyhook controllers can be transformed into the current values with the inverse expression of (25). Details of this transformation are omitted in this paper.

A excitation designed for the simulation is shown in Fig. 5 which consists of random excitations and impact excitations. The expression for this excitation is as follows

$$z_{\mathrm{fr}}(l) = \begin{cases} \text{ISO C} & l \in [0, 20) \\ A_{\mathrm{m1}} \sin((l-20)/L) & l \in [20, 20+L) \\ \text{ISO C} & l \in [20+L, 40+L) \\ A_{\mathrm{m2}} \sin((l-L-40)/2L) & l \in [40+L, 40+3L) \\ \text{ISO C} & l \in [40+3L, 60+3L] \end{cases}$$

where $L = l_f + l_r$, l is the longitudinal displacement, $l = vt$, v is the vehicle speed and A_{mi} $(i = 1, 2)$ are the amplitude of impact roads. For the first impact road, we choose the wavelength equal to L such that the heave motion will be the major response. For the second impact road, the wavelength is set as $2L$ to trigger a pitch response. The random road profiles will trigger both heave and pitch motions and are chosen as the class C road which is suggested by the international standard organization (ISO) and are simulated by the filtering of a white noise. In this paper, we choose $v = 50$km/h and $A_{\mathrm{m1}} = A_{\mathrm{m2}} = 0.2$m.

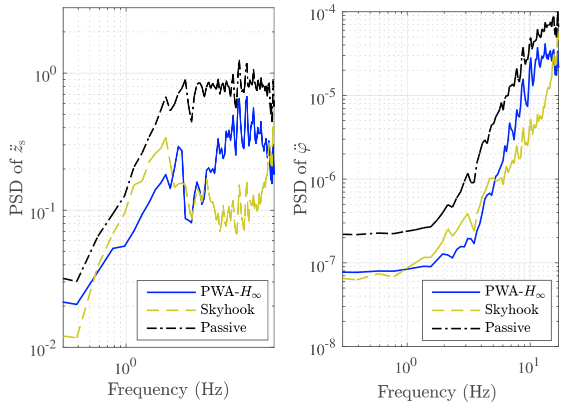

(a) (b)

Fig. 6. PSD results under random road profiles

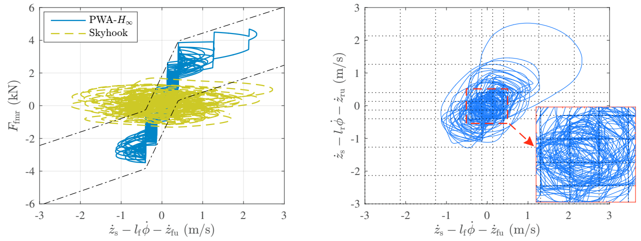

(a) (b)

Fig. 7. Control output and state trajectory

4.2 Results and Analysis

Fig. 6 shows the estimated PSD results of the heave and pitch responses under random road. It has been clearly shown that the proposed PWA-H_∞ controller has evident advantages in a frequency range of 1-4Hz when compared with the Skyhook controller. However, in the higher frequency band, the performance of PWA-H_∞ controller is poorer than that of the Skyhook controller, but improvement with respect to the passive one can still be achieved. Fig. 7 shows the control outputs of different controllers and the transfer of system state under PWA-H_∞ control. Refer to Fig. 7(a), we can see that the output of the proposed PWA-H_∞ controller can satisfy the nonlinear actuator

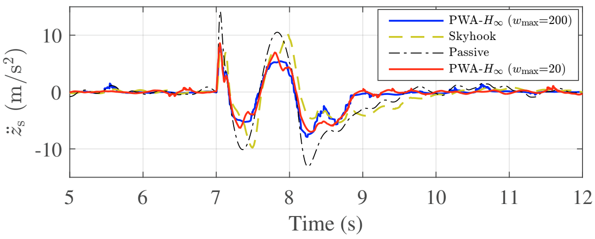

Fig. 8. Responses under heave impact.

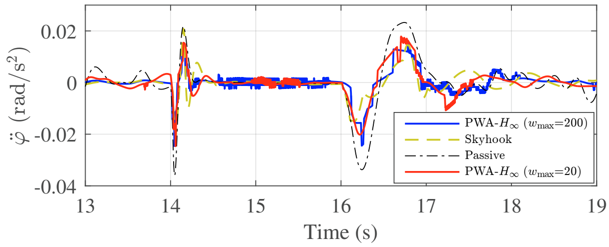

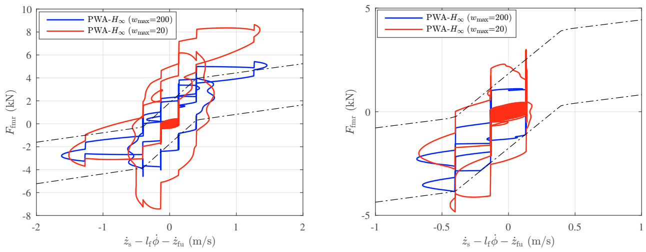

(a) (b)

Fig. 9. Responses under pitch impact.

Fig. 10. Control output ((a):heave impact, (b) pitch impact)

constraint, while that of the Skyhook controller are mostly unavailable. In Fig. 7(b), the system states under PWA-H_∞ control transfer among the designed system regions. However, a insight into the dense regions shows that the state switches frequently occur in the region boundaries, which may influence the system performance and need further analysis in the future works.

Figs. 8 and 9 give the responses of different controllers under heave and pitch impact roads, respectively. Different from the random road simulation where the $w_{\max}$ is only chosen as 20, we simulate the conditions when $w_{\max}$ is set as 20 and 200 for the impact roads. From Figs. 8 and 9, we can see that the proposed PWA-H_∞ controllers have smaller peak values and shorter settling time than the Skyhook controller and the passive suspension. Additionally, the performance of PWA-H_∞ controller when $w_{\max} = 200$ is slightly better than that when $w_{\max} = 20$. This phenomenon can be explained by referring to Fig. 10 where the control output of the two PWA-H_∞ controllers are given and the output of PWA-H_∞ when $w_{\max} = 20$ have located beyond the available region of MR dampers. Above all, we can conclude that although the nonlinear constraint can be handled using the proposed method, but using a single controller to adapt different road profiles will also result in conservatism.

5. CONCLUSION

A novel method to handle the nonlinear actuator of half-car MR suspensions has been given in this paper. The nonlinear control constraints have been approximated by piecewise constant constraints and the state transfer among different system partitions has been defined. Based on the new modeling method, a PWA-H_∞ controller has been given. The simulations under random roads and impact roads have revealed the effectiveness of the proposed method. Future works will focus on the smooth transfer of system state between different partitions and the gain scheduling method for varied road conditions.

REFERENCES

Canale, M., Milanese, M., and Novara, C. (2006). Semi-active suspension control using fast model-predictive techniques. *IEEE Transactions on Control Systems Technology*, 14(6), 1034–1046.

Choi, S.B., Lee, H.K., and Chang, E.G. (2001). Field test results of a semi-active er suspension system associated with skyhook controller. *Mechatronics*, 11(3), 345–353.

Choi, S.B., Li, W., Yu, M., Du, H., Fu, J., and Do, P.X. (2016). State of the art of control schemes for smart systems featuring magneto-rheological materials. *Smart Materials & Structures*, 25(4), 043001.

Csek, L.H., Kvasnica, M., and Lantos, B. (2015). Explicit mpc-based rbf neural network controller design with discrete-time actual kalman filter for semiactive suspension. *IEEE Transactions on Control Systems Technology*, 23(5), 1736–1753.

Du, H., Sze, K.Y., and Lam, J. (2005). Semi-active H_∞ control of vehicle suspension with magneto-rheological dampers. *Journal of Sound & Vibration*, 283(283), 981–996.

Gao, Y., Liu, Z., and Chen, H. (2009). Robust H_∞ control for constrained discrete-time piecewise affine systems with time-varying parametric uncertainties. *IET Control Theory & Applications*, 3(8), 1132–1144.

Giorgetti, N., Bemporad, A., Tsengz, H.E., and Hrovat, D. (2006). Hybrid model predictive control application towards optimal semi-active suspension. *International Journal of Control*, 79(5), 521–533.

Guo, S., Yang, S., and Pan, C. (2006). Dynamic modeling of magnetorheological damper behaviors. *Journal of Intelligent Material Systems & Structures*, 17(1), 3–14.

Huang, Y., Na, J., Wu, X., and Gao, G. (2018). Approximation-free control for vehicle active suspensions with hydraulic actuator. *IEEE Transactions on Industrial Electronics*, PP(99), 1–1.

Pohoryles, D.A. and Duffour, P. (2015). Adaptive control of structures under dynamic excitation using magnetorheological dampers: An improved clipped-optimal control algorithm. *Journal of Vibration & Control.*

Sturm, J.F. (1999). Using sedumi 1.02, a matlab toolbox for optimization over symmetric cones. *Optimization Methods & Software*, 11(1-4), 625–653.

Tseng, H.E. and Hrovat, D. (2015). State of the art survey: active and semi-active suspension control. *Vehicle System Dynamics*, 53(7), 1034–1062.

Wang, D.H. and Liao, W.H. (2011). Magnetorheological fluid dampers: a review of parametric modelling. *Smart Material Structures*, 20(2), 023001.